A Theoretical Investigation of the Bonding of Early Transition Metals to Tellurium *

Nikolas Kaltsoyannis
Chemical Sciences Division, Lawrence Berkeley Laboratory, Berkeley, CA, 94720, USA

Non-relativistic and relativistic discrete variational Xα calculations have been performed on the model complexes $[W(PH_3)_4E_2]$ (E = O, S or Te). The results are consistent with the formal description of the compounds as eighteen-electron tungsten(IV) d^2 systems. Metal–chalcogen σ bonding becomes increasingly covalent as the chalcogen is altered from O to Te, while the almost equal tungsten and chalcogen contributions to the π levels remain more constant. Ligand-based spin–orbit coupling effects are substantial in $[W(PH_3)_4Te_2]$ and smaller for $[W(PH_3)_4S_2]$ and $[W(PH_3)_4O_2]$. Mixing of the σ/π character of the non-relativistic $3a_1$ (W–Te σ) and 3e (Te $5p_\pi$ lone pair) molecular orbitals of $[W(PH_3)_4Te_2]$ occurs in the relativistic calculations. A similar effect is seen in the 1e (W–O π) and $2a_1$ (W–O σ) levels of $[W(PH_3)_4O_2]$. The theoretical results are in good agreement with the experimental electronic absorption spectra of $[W(PMe_3)_4E_2]$ (E = S, Se or Te). The bonding in the model complex $[Zr(TeSiH_3)_4]$ is discussed in conjunction with the closely related ZrI_4. The separation of the metal–ligand σ and π levels is significantly greater in the tellurium compound. Previous predictions for the spin–orbit splitting of the $t_2(\sigma)$ and $t_2(\pi)$ subshells of Group IVA tetrahalides are reproduced more closely in $[Zr(TeSiH_3)_4]$ than in ZrI_4, in which there is substantial $t_2(\sigma)$–$t_2(\pi)$ mixing. Attempts to assign the valence photoelectron spectra of MX_4 (M = Ti, Zr or Hf; X = Br or I) in terms of the earlier theoretical model are considered to be inappropriate in light of the lack of $t_2(\sigma)$–$t_2(\pi)$ separation. Comparison of the metal–tellurium bonding in $[W(PH_3)_4Te_2]$ with that in $[Zr(TeSiH_3)_4]$ suggests that the former is significantly more covalent.

In the last few years there has been considerable interest in the synthesis and characterisation of compounds containing terminal metal–ligand multiple bonds.[1,2] Chalcogens (E) have received particular attention, due in part to the potential role of metal chalcogenides in thin-film semiconductors.[3] Terminally bound M–E species are believed to be intermediates in the decomposition of monomeric precursors to bulk materials.[4] With the greater tendency of heavier main-group elements to bridge two or more metal centres,[5,6] terminally bound M–E (E = Se or Te) species provide a substantial synthetic challenge. The first transition-metal complex with a terminal tellurido ligand, $[W(PMe_3)_4Te_2]$, was reported only very recently by Rabinovich and Parkin,[7] and the sulfur[8] and selenium[9] analogues have also been prepared. Christou and Arnold[4] have reported the synthesis of $[ZrTe\{TeSi(SiMe_3)_3\}_2(dmpe)_2]$ (dmpe = $Me_2PCH_2CH_2PMe_2$) which contains both single and double metal–tellurium bonds.

The electronic structure of these compounds is particularly interesting in that Te occupies a position intermediate between the very electronegative elements in the upper right-hand part of the Periodic Table and the transition metals. Furthermore, it is a sufficiently heavy atom that ligand-based spin–orbit coupling effects are expected to be significant, in addition to those arising from the transition metal. The fully relativistic implementation of the discrete variational (DV) Xα method of Ellis[10] employed in this study is well suited to probing the effects of spin–orbit coupling, and has enjoyed significant success in addressing the electronic structures of complexes containing heavy elements.[11–14]

Two compound types are discussed in this paper. Those of $[W(PH_3)_4E_2]$ (E = O, S or Te) provide an opportunity to address not only W–Te multiple bonding, but also to investigate bonding trends as the chalcogen is altered. Comparison is made between the theoretical results and the experimental electronic absorption spectra of $[W(PMe_3)_4E_2]$ (E = S, Se or Te).[15] The compound $[Zr(TeSiH_3)_4]$ is used as a model for $[Zr\{TeSi(SiMe_3)_3\}_4]$, which is a stable intermediate in the preparation of $[ZrTe\{TeSi(SiMe_3)_3\}_2(dmpe)_2]$.[4] The formally singly bonded $[Zr(TeSiH_3)_4]$ provides a comparison with the W–Te multiple bond, and also with the closely related ZrI_4. The effects of spin–orbit coupling on the electronic structures of the Group IVA tetrahalides are still not fully understood, particularly in relation to their photoelectron spectra.[16–19] It is hoped that a comparative study of ZrI_4 and $[Zr(TeSiH_3)_4]$ can help to resolve this twenty-five year old problem.

Theoretical Considerations and Computational Details

There are two major consequences of relativity for the chemistry of systems containing one or more heavy elements. The first is the significant modification of the valence atomic orbital (AO) energies as a result of the stabilisation of the inner core s and p electrons, which are moving at velocities which are appreciable fractions of the speed of light. The effect on the valence orbitals is to contract slightly the s and p levels and to destabilise the more diffuse d and f functions, which experience reduced nuclear charge due to increased shielding by the s and p electrons.[20]

The second consequence is the coupling of the electron's intrinsic spin angular momentum with that imposed by its orbital motion, an effect which is increasingly important for heavy-element systems. All electronic states in heavy-element complexes are therefore properly characterised by non-integral angular momentum values, and must be described using double point-group symmetry notation.[21]

It is therefore necessary to incorporate relativistic corrections into the molecular Hamiltonian for heavy-element

* *Supplementary data available* (No. SUP 57000, 13 pp.): molecular orbital eigenvalues and atomic compositions. See Instructions for Authors, *J. Chem. Soc., Dalton Trans.*, 1994, Issue 1, pp. xxiii–xxviii.

Non-SI unit employed: eV ≈ 1.60×10^{-19} J.

systems. The details of the relativistic DV-Xα method employed in this work have been given elsewhere,[11,12] and only a brief summary is provided here. The approach incorporates the Dirac operator into the traditional Hartree–Fock treatment, the molecular wavefunction being represented as a Slater determinant over four-component one-electron wavefunctions. Application of the variation principle to this antisymmetrised wavefunction yields the Dirac–Fock one-electron equations, analogous to the non-relativistic case.[22,23] The Dirac–Fock equations contain both relativistic one-electron terms and non-relativistic two-electron terms corresponding to electrostatic electron–electron repulsions. The latter terms were replaced by a coulomb repulsion operator and an approximate local-density-functional exchange-correlation operator. The simplest choice for this operator is Slater's Xα potential,[24,25] although the improved parameterisation of Hedin and Lundqvist[26] has been employed in the calculations reported here.

The molecular orbitals (MOs) were expressed as a linear combination of atomic orbitals expansion in a basis of symmetry-adapted four-component atomic functions. The large and small radial components were obtained from numerical atomic Dirac–Fock–Slater calculations, performed on neutral atoms and cations and subsequently combined to provide a 'multi-zeta' basis of approximately split valence quality. The self-consistent multipolar charge-density representation was used in evaluating the molecular coulomb integrals.[27] A Mulliken population analysis[28] was employed in order to provide an approximate estimation of the molecular charge density.

The bond lengths used in the calculations of the model complexes $[W(PH_3)_4E_2]$ were taken from crystal structure data where possible. In all cases the W–P and P–H bond lengths were held constant, at 2.508[7] and 1.42 Å respectively. The W–E distances employed were 2.596 Å for E = Te[7] and 2.248 Å for E = S.[8] The oxygen analogue of these compounds has not yet been synthesised,[9] and the W–O bond length used was 1.71 Å, this being the distance in $[W(O)Cl_2(CH_2CH_2)(PMePh_2)_2]$[29] and also in OsO_4.[30]

For $[Zr(TeSiH_3)_4]$ the Zr–Te and Te–Si bond lengths were taken from the crystal structure of $[Zr\{TeSi(SiMe_3)_3\}_4]$,[4] at 2.74 and 2.40 Å respectively; Si–H was estimated from ionic radii data,[31] at 1.40 Å. The Zr–I bond length in ZrI_4 was taken to be the same as the Zr–Te distance in $[Z(TeSiH_3)_4]$ for comparative purposes.

In all cases the molecular symmetry was idealised to the highest possible, C_{4v} for $[W(PH_3)_4E_2]$ and T_d for $[Zr(TeSiH_3)_4]$ and ZrI_4.

All density-functional calculations were performed on the Cray Y-MP8 supercomputer at the Ohio Supercomputing Centre. The results are presented pictorially *via* energy-level diagrams and contour plots. Tabulated MO eigenvalues and percent AO compositions are available as supplementary material (SUP 57000).

The AO energies discussed in the final section of the paper were taken from Hartree–Fock SCF calculations using the RCN program (version 36) of Cowan.[32] Mass-velocity and Darwin corrections were included in the differential equations to obtain the relativistic AO energies. The calculations were performed on a Sun Sparcserver 630MP workstation.

Results and Discussion

Compounds $[W(PH_3)_4E_2]$ (E = O, S *or* Te).—In the first part of this paper the electronic structure of $[W(PH_3)_4E_2]$ is investigated. A bonding model for $[W(PH_3)_4Te_2]$ is set up at the non-relativistic level, followed by a comparison of $[W(PH_3)_4S_2]$ and $[W(PH_3)_4O_2]$ with their heavier congenor. In particular, the MO description of the eighteen-electron nature of these compounds and the degree of covalency in the W–E bonding orbitals is addressed. Subsequently the same three compounds are studied by relativistic calculations. The compound $[W(PH_3)_4S_2]$, for which chalcogen-based spin–orbit coupling effects are expected to be small, is used to relate non-relativistic and relativistic MO schemes. The larger spin–orbit couplings in $[W(PH_3)_4Te_2]$ are then investigated, and a comparison of all three molecules at the relativistic level is provided. Finally, a comparison is made of the ground-state orbital energies of $[W(PH_3)_4E_2]$ (E = O, S or Te) with the electronic absorption spectra of $[W(PMe_3)_4E_2]$ (E = S, Se or Te).[15]

(*a*) *Non-relativistic calculations.* (*i*) $[W(PH_3)_4Te_2]$. This compound is an example of the *trans*-dielement ligand configuration, which has been shown to give rise to an axially compressed ligand field.[33–35] Although the highest possible symmetry of $[W(PH_3)_4Te_2]$ is C_{4v}, it is anticipated that many of the familiar features of the MO structure of octahedral transition-metal complexes[36] will be present in the *trans*-dielement system. If the Te–W–Te axis is taken to be the *z* axis, the metal–ligand orbital interactions that are confined to the *xy* plane may be expected to be little perturbed from those in a genuinely octahedral complex.

In C_{4v} symmetry the four W–P σ bonds transform as $a_1 + b_1 + e$. Fig. 1 indicates that at most negative eigenvalues among the valence MOs* are found the $1a_1$–$1e$ levels, which are indeed W–P σ bonding. This is illustrated in Fig. 2(*a*), which shows a contour plot of the $1b_1$ MO in the *xy* plane. It is interesting that both W 6s and 6p AOs are involved in W–P bonding, in addition to the 5d (the $1a_1$ MO has *ca.* 14% W 6s character, and a similar 6p contribution is found in the 1e level). In particular, the metal 6p contribution to the 1e MO has a significant effect in the relativistic calculations [see below, section (*b*)(*ii*)].

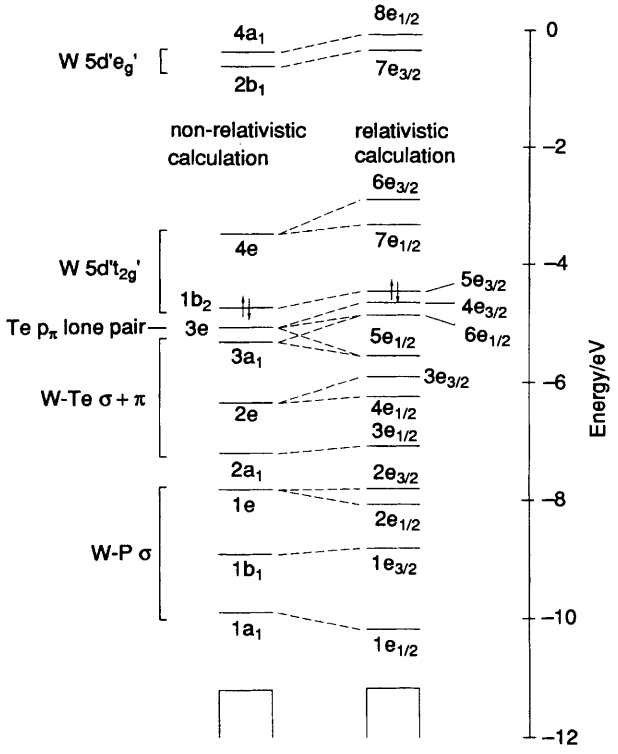

Fig. 1 Non-relativistic and relativistic molecular orbital energy-level diagram for $[W(PH_3)_4Te_2]$

* For the purposes of this and subsequent discussion, the valence MOs are considered to be those with metal–ligand bonding or antibonding character, or non-bonding levels occurring in the same energy range. Hence the large number of P–H bonding MOs, all of which have more negative eigenvalues than that of the $1a_1$ level, are not included in the valence set.

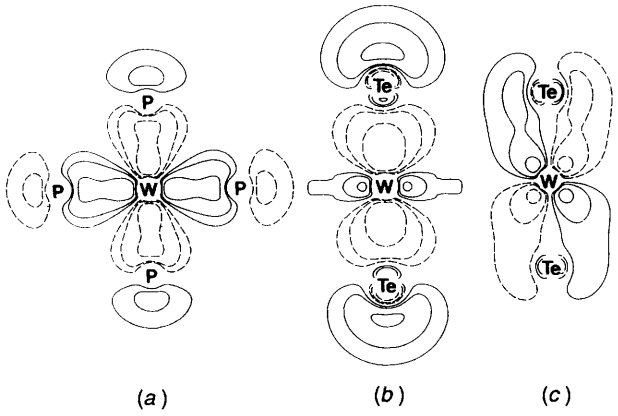

Fig. 2 Contour plots of the (*a*) $1b_1$ (*xy* plane), (*b*) $2a_1$ (*xz* plane) and (*c*) 2e (σ_d plane) non-relativistic molecular orbitals of $[W(PH_3)_4Te_2]$

The two W–Te vectors both transform as a_1 in C_{4v} symmetry, which indicates that W–Te σ bonding is confined to MOs of a_1 symmetry. From the tellurium standpoint one of these a_1 levels corresponds to the two Te $5p_z$ AOs being in phase with one another while the other has them out of phase. The former is the $2a_1$ complex MO, illustrated in Fig. 2(*b*), in which the in-phase $5p_z$ interaction is significantly stabilised by interaction with the W $5d_{z^2}$ AO. The $2a_1$ MO is therefore seen to be highly delocalised and strongly W–Te σ bonding. The remaining filled a_1 MO, the $3a_1$, is much more Te-localised and corresponds to the out-of-phase Te $5p_z$ combination. There is a small W 6p contribution to this MO which imparts some metal–ligand bonding, but overall the $3a_1$ MO is much less W–Te bonding than is the $2a_1$. This is reflected in the energy gap between these orbitals, some 1.90 eV.

The 2e MO, which lies in between the $2a_1$ and $3a_1$, is highly delocalised over the Te–W–Te vector and is strongly π bonding. One component is shown in Fig. 2(*c*). In contrast, the 3e MO is almost exclusively Te-localised (88.65%), and is Te $5p_\pi$ lone pair in character. Of the $2a_1$–3e MOs, W–Te bonding is concentrated in the $2a_1$ and 2e (in which it is very covalent) with a small contribution from the $3a_1$. The 3e level is W–Te non-bonding.

The complex highest-occupied MO (HOMO), the $1b_2$ orbital, is found to be 86.24% W $5d_{xy}$ in character. This is in agreement with the previous description of $[W(PMe_3)_4Te_2]$ as a tungsten(VI) d^2 system.[7] In this work it was also noted that in order to satisfy the eighteen-electron rule the W–Te bond order is restricted to two. Lone-pair donation from Te to W (*i.e.* $^-W{\equiv}Te^+$) would increase the formal tungsten electron count above eighteen and is therefore prohibited.

An MO equivalent of this description may be obtained by an examination of the $1a_1$–$1b_2$ valence levels. Orbitals $1a_1$–1e contain the eight W–P σ-bonding electrons. The $2a_1$ and $3a_1$ levels contribute four W–Te σ electrons, although the extent of metal–ligand bonding is much greater in the $2a_1$. Four more electrons in the 2e W–Te π bonding MO brings the count to sixteen. The two electrons in the $1b_2$ HOMO therefore complete the eighteen-electron count and the electrons in the 3e MO have not been included. The tellurium localisation and almost complete lack of metal character in the 3e level are the MO equivalent of there being no Te→W lone-pair donation. The analogy is not perfect in that there are varying degrees of metal involvement in the valence MOs which are considered to contribute to the eighteen-electron count, but the 3e orbital has almost no tungsten content (1.95%).

In a σ-only octahedral ligand field, transition-metal d orbitals split into the familiar three-below-two pattern, with the metal–ligand σ^* e_g orbitals being destabilised above the non-bonding t_{2g} set.[36] The $1b_2$–$4a_1$ MOs of $[W(PH_3)_4Te_2]$ illustrate how this splitting is modified when two of the six ligands are replaced with a *trans* arrangement of π donors (assuming the PH_3 ligands to be only σ donors). The non-bonding t_{2g} set is split into b_2 and e levels. The former remains non-bonding as the d_{xy} orbital has no interaction with the Te atoms. The d_{xz} and d_{yz} orbitals, however, are destabilised by a π interaction with the tellurium ligands. The $1b_2$ and 4e MOs of $[W(PH_3)_4Te_2]$ are therefore related to the metal d-based t_{2g} orbitals of an octahedral complex. The $1b_2$ HOMO is essentially tungsten-localised while the 4e lowest-unoccupied MO (LUMO) is W–Te π^* in character.

The $2b_1$ and $4a_1$ MOs are the C_{4v} equivalents of the metal–ligand σ^* e_g MOs of a σ-only octahedral complex. The W–P σ antibonding character is distributed among both orbitals, while the W–Te σ^* interaction is restricted to the $4a_1$ level. Both the $2b_1$ and $4a_1$ MOs are appreciably higher in energy than are the $1b_2$ and 4e. Hence the overall three-below-two spread of metal d-based orbitals is retained in $[W(PH_3)_4Te_2]$, although the degeneracies of both groups are lifted by the C_{4v} ligand field.

It is worth noting how the $1a_1$–$4a_1$ MOs of $[W(PH_3)_4Te_2]$ are grouped according to the type of metal–ligand interaction present in each. At most negative eigenvalues come the W–P σ bonding levels, followed by the W–Te σ + π orbitals, the lone-pair orbitals of Te and W and finally the W–Te and W–P antibonding levels. All of the MOs up to and including the non-bonding levels are filled.

(*ii*) *Comparison of* $[W(PH_3)_4S_2]$ *and* $[W(PH_3)_4O_2]$ *with* $[W(PH_3)_4Te_2]$. Although the overall orbital structure of $[W(PH_3)_4S_2]$ and $[W(PH_3)_4O_2]$ is expected to be similar to that of $[W(PH_3)_4Te_2]$, the markedly different energies and radial extensions of the 2p, 3p and 5p chalcogen AOs should give rise to some interesting trends. The results of the non-relativistic calculations on $[W(PH_3)_4S_2]$ and $[W(PH_3)_4O_2]$ are given in Figs. 3 and 4 {the unoccupied levels of $[W(PH_3)_4O_2]$ lie too high in energy to be conveniently displayed}, while Fig. 5 provides a comparison of the valence MO energies of $[W(PH_3)_4E_2]$ (E = S, O or Te).

The MO ordering of $[W(PH_3)_4S_2]$ is similar to that of $[W(PH_3)_4Te_2]$, the only change being the stabilisation of the W–E σ bonding $2a_1$ MO below the W–P σ bonding 1e level. Indeed, the W–P bonding $1a_1$, $1b_1$ and 1e MOs are little altered from $[W(PH_3)_4Te_2]$ in both composition and energy. More significant differences occur in the $2a_1$ and 2e orbitals, which are 0.86 and 0.85 eV respectively more stable than the equivalent W–Te σ- and π-bonding orbitals. Slight stabilisation of the $3a_1$–$1b_2$ MOs are found in $[W(PH_3)_4S_2]$, and their compositions are very similar to those of the tellurium analogues. Once again the calculation indicates that the HOMO is the W $5d_{xy}$ $1b_2$ level, and that $[W(PH_3)_4S_2]$ may also be described as a tungsten(IV) d^2 system.

In contrast, $[W(PH_3)_4O_2]$ is appreciably different from $[W(PH_3)_4S_2]$ and $[W(PH_3)_4Te_2]$. As may be expected, this is most apparent in the W–O bonding levels, particularly the 1e π MO. While the $2a_1$ W–O σ orbital is stabilised by 0.34 eV from its $[W(PH_3)_4S_2]$ counterpart, the 1e π level is 1.43 eV more stable. Indeed the W–E σ-bonding MO lies 0.87 eV below the π level in $[W(PH_3)_4Te_2]$ and 0.89 eV in $[W(PH_3)_4S_2]$ whereas in $[W(PH_3)_4O_2]$ the π MO is 0.20 eV more stable than the σ. This situation is reminiscent of OsO_4, in which the Os–O π-bonding e MO is found both theoretically and experimentally to be almost isoenergetic with the Os–O σ t_2 level.[14,30,37] Metal–ligand π interactions are more sensitive to bond lengths than are σ effects, and it is likely that this is a major factor in determining the relative W–E σ and π MO energies in $[W(PH_3)_4E_2]$.

There is a greater mixing of E and P character in some of the valence levels of $[W(PH_3)_4E_2]$ as E moves from Te to O. There is only 4.68% Te character to the W–P σ-bonding 1e MO of $[W(PH_3)_4Te_2]$, but this rises to 9.77% in $[W(PH_3)_4S_2]$ and to 16.56% in the 2e level of $[W(PH_3)_4O_2]$. An opposite trend is observed in the 3e E p_π lone-pair MO, in which the phosphorus character increases from 6.31% in $[W(PH_3)_4Te_2]$ to 18.72% in $[W(PH_3)_4O_2]$. The $1b_2$ MO can have no chalcogen character

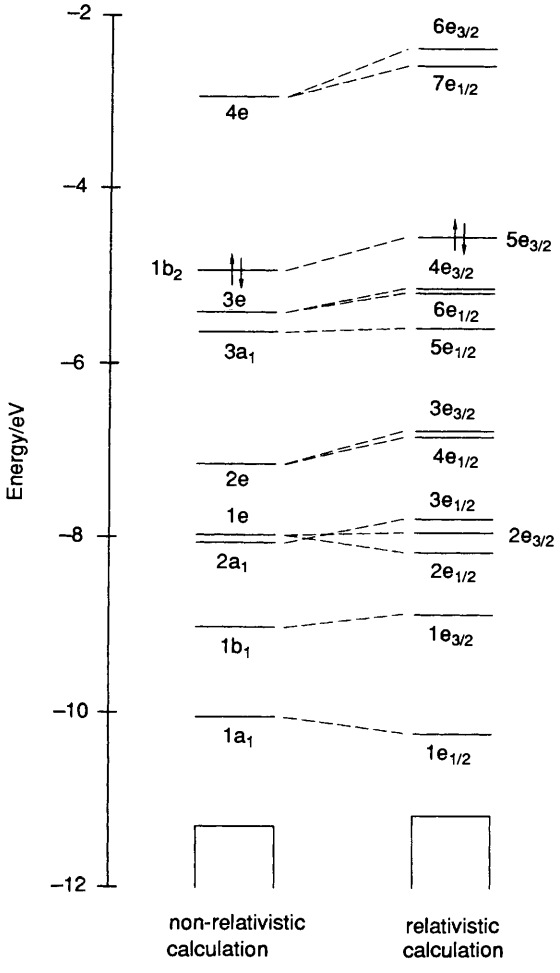

Fig. 3 Non-relativistic and relativistic molecular orbital energy-level diagram for $[W(PH_3)_4S_2]$

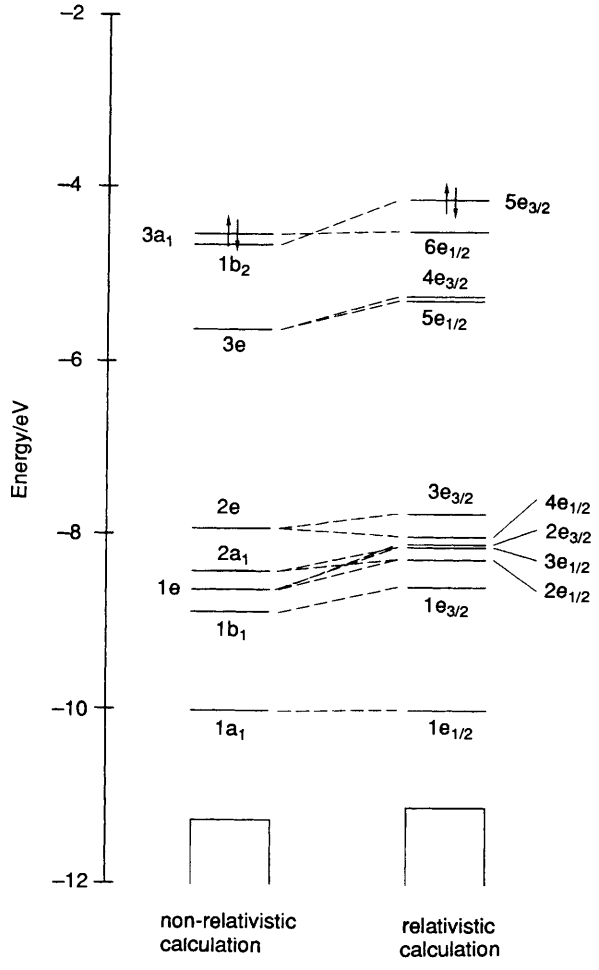

Fig. 4 Non-relativistic and relativistic molecular orbital energy-level diagram for $[W(PH_3)_4O_2]$

by symmetry, and its energy and composition are little different in the three calculations. However, while it is the HOMO of both $[W(PH_3)_4Te_2]$ and $[W(PH_3)_4S_2]$, the calculation on $[W(PH_3)_4O_2]$ predicts that the $3a_1$ W–O bonding MO is destabilised above it. This MO has significant E–E antibonding character, and the much closer proximity of the chalcogen atoms in $[W(PH_3)_4O_2]$ results in a strengthening of the effect. The small stabilising W 6p contribution is insufficient to prevent the $3a_1$ level from becoming the HOMO of $[W(PH_3)_4O_2]$.

Of key interest is the degree of metal–chalcogen covalency in the three complexes. Focusing on the MOs responsible for the major part of the W–E bonding, the $2a_1$ (σ) and 2e {π, 1e in $[W(PH_3)_4O_2]$}, it is found that there is a marked increase in covalency in the former as the chalcogen becomes heavier. This is illustrated in Fig. 6, which plots the contributions of W and E to the σ- and π-bonding MOs in the three complexes. The tungsten character of the σ MO increases from 12.71% in $[W(PH_3)_4O_2]$ to 29.49% in $[W(PH_3)_4S_2]$ and 38.06% in $[W(PH_3)_4Te_2]$, with concomitant reduction of the contribution of E from 77.44 to 67.80 and 58.75%. In contrast, the relative metal and chalcogen contributions to the π levels remain much more constant between $[W(PH_3)_4E_2]$ (E = O, S or Te), although the trend is the same. The Allred–Rochow electronegativities of the chalcogens are 3.50 for O, 2.44 for S and 2.01 for Te, with that of W being 1.40.[31] The degree of covalency in the W–E bonding indicated by the calculations follows the trend expected from the difference in electronegativity between metal and ligand.

(*b*) *Relativistic calculations.* For $[W(PH_3)_4E_2]$ (E = O or S)

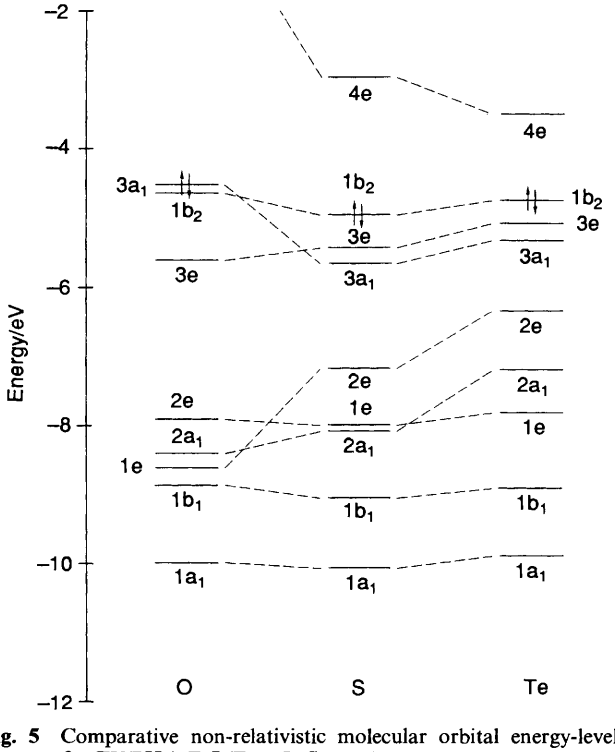

Fig. 5 Comparative non-relativistic molecular orbital energy-level diagram for $[W(PH_3)_4E_2]$ (E = O, S or Te)

the only significant effects of the incorporation of relativistic quantum mechanics into the calculational procedure will be upon MOs with appreciable tungsten character. Oxygen and sulfur are light elements, and the relativistic modifications of their AO energies and the extent of spin–orbit coupling are small. In contrast, significant differences between the non-relativistic and relativistic calculations on $[W(PH_3)_4Te_2]$ may be expected in both metal- and chalcogen-based MOs. The C_{4v}* double group has two irreducible representations in addition to those of the single group, and all electronic states in relativistic $[W(PH_3)_4E_2]$ carry either the $e_{1/2}$ or the $e_{3/2}$ symmetry labels. The relationship between the spatial MOs of the C_{4v} point group and the spin orbitals of C_{4v}* are given in Table 1.

(*i*) $[W(PH_3)_4S_2]$. Of the relativistic calculations that on $[W(PH_3)_4S_2]$ is most clearly related to its non-relativistic analogue, and as such provides the best starting point for the following discussion. The results are given on the right-hand side of Fig. 3.

The ordering of orbital type is very much as for the non-relativistic approach, the only difference being the destabilisation of the $3e_{1/2}$ ($2a_1$) MO above the $2e_{1/2}$ and $2e_{3/2}$ (1e) levels. This gives relativistic $[W(PH_3)_4S_2]$ the same energetic division of MOs into bonding type seen in non-relativistic $[W(PH_3)_4Te_2]$.

The differences in relativistic and non-relativistic W–P bonding MOs are readily understood by consideration of their tungsten character. The $1e_{1/2}$ level is slightly more stable than the $1a_1$, on account of its 9.24% W 6s content. In contrast, the contribution of W to the $1e_{3/2}$ MO is exclusively 5d and $5\bar{d}$,† resulting in the relativistic MO being destabilised with respect to the $1b_1$ level. The 1e non-relativistic MO is split by spin–orbit coupling into the $2e_{1/2}$ and $2e_{3/2}$ levels. The size of this splitting, 0.27 eV, is not great, but is significantly bigger than that of the $6e_{1/2}$ and $4e_{3/2}$ (3e) levels. These latter MOs are almost entirely S-based and their splitting is minimal. It is therefore likely that the spin–orbit splitting of the $2e_{1/2}$ and $2e_{3/2}$ MOs is due to their *ca.* 15% W 6p and $6\bar{p}$ content, as any P-induced splitting will be similar to that of S. The spin–orbit splittings due to the 3p AOs of P and S will be very similar to that of Cl, for which the spin–orbit coupling of the $3p^5$ configuration is particularly simple.

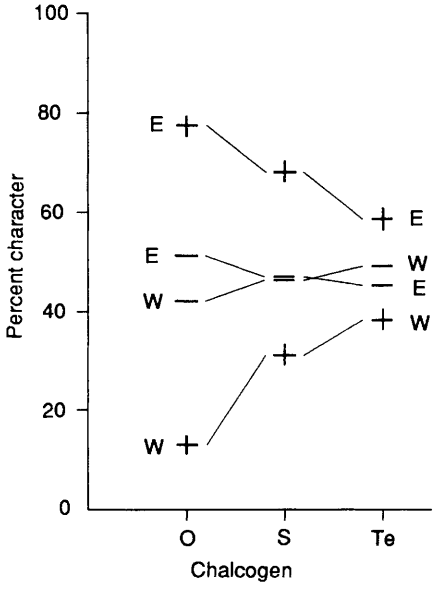

Fig. 6 Metal and chalcogen character of the W–E σ- and π-bonding molecular orbitals (+ and −) of $[W(PH_3)_4E_2]$ (E = O, S or Te)

† A bar orbital label ($\bar{d}$ for example) refers to the lower angular momentum component of the spin–orbit coupled atomic orbitals and an unbarred orbital refers to the higher angular momentum component.

Experimentally the splitting between the $^2P_{1/2}$ and $^2P_{3/2}$ levels of Cl is 881 cm^{-1},[38] or 0.109 eV, and it is very unlikely that any S- or P-induced splitting will be greater than this.

The $3e_{1/2}$ and ($4e_{1/2}$ + $3e_{3/2}$) MOs are destabilised with respect to their non-relativistic counterparts, the $2a_1$ and 2e W–S bonding levels. This is due to their substantial W (5d + $5\bar{d}$), content, which is similar to that found in the non-relativistic levels. Although there is strictly no σ/π separability in the $e_{1/2}$ and $e_{3/2}$ MOs, the principal metal–ligand interactions are retained in the relativistic calculations. This is illustrated in Fig. 7, which shows contour plots of the normalised squares of the $3e_{1/2}$ and $4e_{1/2}$ MOs. Note that the $2e_{1/2}$ and $2e_{3/2}$ MOs have about one third of the tungsten content of the $4e_{1/2}$ and $3e_{3/2}$, and yet their splitting is nearly three times as great. This is in accord with p-based spin–orbit coupling being greater than d-based.[39]

The $5e_{1/2}$ is the relativistic equivalent of the $3a_1$ level, which is W–S bonding by virtue of a small metal 6p and $6\bar{p}$ contribution. The $6e_{1/2}$ and $4e_{3/2}$ MOs are sulfur lone pair in character, which makes their slight destabilisation above the 3e non-relativistic MO difficult to explain. It is unlikely that their small tungsten content is sufficient to produce the effect.

There are two electrons in the $5e_{3/2}$ HOMO, which is 84.93% W (5d + $5\bar{d}$) in character. Thus the relativistic calculation is in agreement with the non-relativistic in finding $[W(PH_3)_4S_2]$ to be a d^2 system. The LUMO and next LUMO are W–S π* in character and are related to the 4e non-relativistic LUMO. Overall, therefore, the relativistic calculation yields results in close agreement with the non-relativistic. The small shifts in orbital energies can be rationalised largely in terms of the tungsten AO content of the MOs, and the spin–orbit splittings of the e-symmetry non-relativistic orbitals are not great.

(*ii*) $[W(PH_3)_4Te_2]$. The relativistic results on $[W(PH_3)_4Te_2]$ are given on the right-hand side of Fig. 1. They are broadly similar to the non-relativistic and to the results obtained for $[W(PH_3)_4S_2]$, and where differences do occur they can be traced

Table 1 Relationship between the irreducible representations of C_{4v} and C_{4v}*, T_d and T_d*

C_{4v}	C_{4v}*	T_d	T_d*
a_1	$e_{1/2}$	a_1	$e_{1/2}$
a_2	$e_{1/2}$	a_2	$e_{5/2}$
b_1	$e_{3/2}$	e	$g_{3/2}$
b_2	$e_{3/2}$	t_1	$g_{3/2}$ + $e_{1/2}$
e	$e_{1/2}$ + $e_{3/2}$	t_2	$g_{3/2}$ + $e_{5/2}$

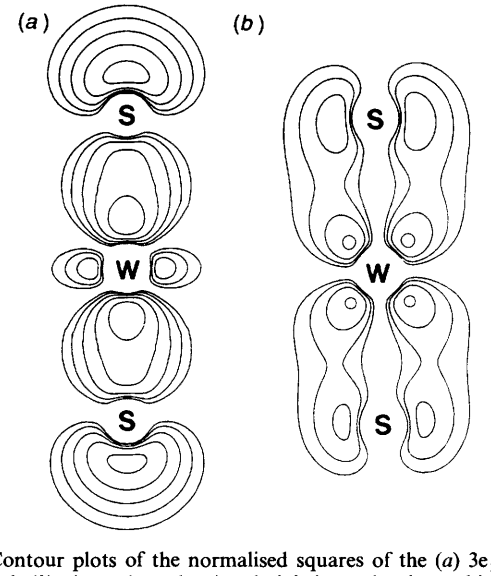

Fig. 7 Contour plots of the normalised squares of the (*a*) $3e_{1/2}$ (*xz* plane) and (*b*) $4e_{1/2}$ (σ_d plane) relativistic molecular orbitals of $[W(PH_3)_4S_2]$

to the increase in chalcogen-based spin–orbit coupling. The $1e_{1/2}$–$2e_{3/2}$ W–P levels are similar to the $[W(PH_3)_4S_2]$ equivalents, although there is a slightly reduced tungsten content to the $1e_{1/2}$ MO. The spin–orbit splitting of the $2e_{1/2}$ and $2e_{3/2}$ orbitals is almost identical in $[W(PH_3)_4S_2]$ and $[W(PH_3)_4Te_2]$, in accord with their very similar AO compositions.

The first significant difference comes in the separation of the $4e_{1/2}$ and $3e_{3/2}$ MOs, which are W–E π bonding. Their relative W/E content is the same in both $[W(PH_3)_4S_2]$ and $[W(PH_3)_4Te_2]$, yet the energy gap between them is three and a half times as great in the tellurium compound. This is clearly due to the increased spin–orbit coupling induced by the heavier chalcogen. A similar situation exists for the $7e_{1/2}$ and $6e_{3/2}$ unoccupied MOs, which have significantly greater separation in the tellurium compound while having similar W/E AO character in both $[W(PH_3)_4S_2]$ and $[W(PH_3)_4Te_2]$.

The HOMO of relativistic $[W(PH_3)_4Te_2]$ is the $5e_{3/2}$ orbital, which is 84.09% W (5d + 5d̄) in character and again reflects the tungsten(IV) nature of the compound. The $5e_{1/2}$–$4e_{3/2}$ MOs, however, cannot be so clearly related to their $3a_1$ and 3e non-relativistic equivalents, or to their counterparts in $[W(PH_3)_4S_2]$. This is illustrated in Fig. 8, which shows the $5e_{1/2}$, $6e_{1/2}$ and $4e_{3/2}$ MOs of both $[W(PH_3)_4S_2]$ and $[W(PH_3)_4Te_2]$. In the former, the $6e_{1/2}$ and $4e_{3/2}$ MOs are S p_π lone pair in character, while the $5e_{1/2}$ is metal–chalcogen σ bonding. In $[W(PH_3)_4Te_2]$, however, a scrambling of the σ/π nature of the $5e_{1/2}$ and $6e_{1/2}$ MOs has occurred, to the extent that neither level is clearly σ nor π. The AO compositions of these MOs is also very different in $[W(PH_3)_4S_2]$ and $[W(PH_3)_4Te_2]$. In $[W(PH_3)_4S_2]$ both $5e_{1/2}$ and $6e_{1/2}$ are a mixture of S 3p and 3p̄ character while in $[W(PH_3)_4Te_2]$ the $5e_{1/2}$ is predominantly Te 5p̄ and the $6e_{1/2}$ Te 5p. It would therefore appear that the spin–orbit coupling of the Te 5p AOs is the dominant factor in determining the nature of the $5e_{1/2}$ and $6e_{1/2}$ levels of $[W(PH_3)_4Te_2]$, while in $[W(PH_3)_4S_2]$ the much smaller S 3p AO splittings are insufficient to alter the non-relativistic σ/π character. The tie lines from the $3a_1$ and 3e MOs to both the $5e_{1/2}$ and $6e_{1/2}$ levels on Fig. 1 imply that the relativistic orbitals have characteristics of both σ and π non-relativistic MOs.

(iii) $[W(PH_3)_4O_2]$. The relativistic calculation on $[W(PH_3)_4O_2]$ is similar to that on $[W(PH_3)_4S_2]$ in having no significant ligand-derived spin–orbit coupling. The results are given on the right-hand side of Fig. 4.

Unlike $[W(PH_3)_4E_2]$ (E = S or Te), there is no stabilisation of the $1e_{1/2}$ W–P σ-bonding MO over the $1a_1$ level. This may be traced to there being no W 6s content in the $1e_{1/2}$ MO in $[W(PH_3)_4O_2]$. The $1e_{3/2}$ orbital is also W–P σ bonding, with atomic contributions little altered from those of the non-relativistic calculation.

The W–O bonding $2e_{1/2}$–$2e_{3/2}$ orbitals are more stable than the W–P bonding $4e_{1/2}$ and $3e_{3/2}$ levels, as in the non-relativistic calculation. The energy gap between them, however, decreases as a result of the destabilising W (5d + 5d̄) contribution to the $2e_{1/2}$–$2e_{3/2}$ MOs. The spin–orbit splitting of the $4e_{1/2}$ and $3e_{3/2}$ MOs is very similar to that of the equivalent W–P bonding orbitals of $[W(PH_3)_4S_2]$ and $[W(PH_3)_4Te_2]$.

Fig. 9 shows contour plots of the $2e_{1/2}$, $3e_{1/2}$ and $2e_{3/2}$ levels of $[W(PH_3)_4O_2]$. It can be seen that while the $2e_{3/2}$ MO is W–O π in character, there is no clear division of the $2e_{1/2}$ and $3e_{1/2}$ levels into σ and/or π. This is reflected in the atomic compositions of the orbitals. The non-relativistic W–O π-bonding 1e MO has 41.79% tungsten character whereas the $2a_1$ σ level has only 12.71%. The $2e_{3/2}$ π MO has a 38.51% metal contribution, little changed from the non-relativistic case. The $2e_{1/2}$ and $3e_{1/2}$ MOs, however, have 30.95 and 21.00% tungsten content respectively, compositions which are intermediate between the tungsten contributions to the non-relativistic σ and π levels. The contribution *per orbital* [the sum of the tungsten content in the $2a_1$ + 1e (×2) and $2e_{1/2}$ + $3e_{1/2}$ + $2e_{3/2}$ MOs divided by three] to the W–O bonding levels is similar in non-relativistic and relativistic calculations, at 32.10 and 30.15% respectively.

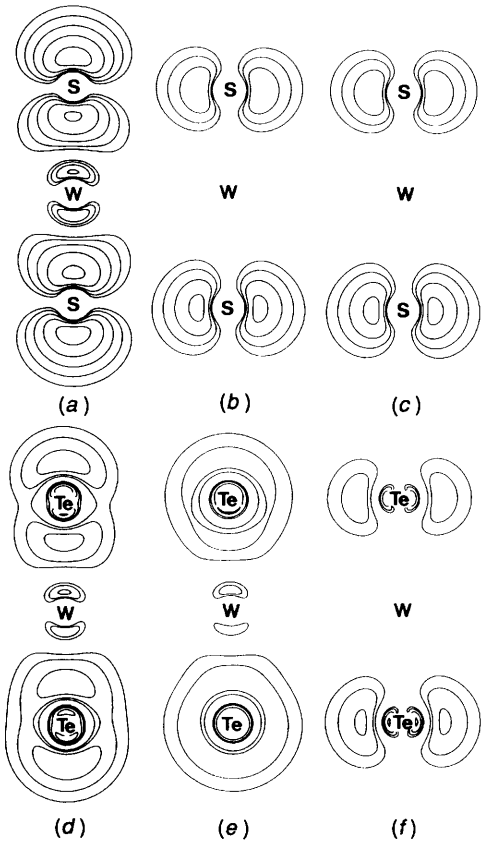

Fig. 8 Contour plots of the normalised squares of the (*a*) $5e_{1/2}$ (*xz* plane), (*b*) $6e_{1/2}$ (σ_d plane) and (*c*) $4e_{3/2}$ (σ_d plane) relativistic molecular orbitals of $[W(PH_3)_4S_2]$ and (*d*) $5e_{1/2}$ (*xz* plane), (*e*) $6e_{1/2}$ (σ_d plane) and (*f*) $4e_{3/2}$ (σ_d plane) relativistic molecular orbitals of $[W(PH_3)_4Te_2]$

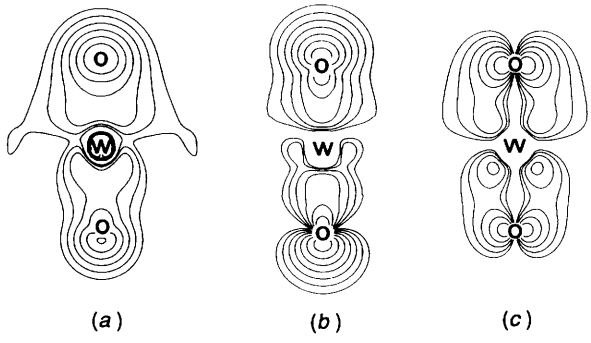

Fig. 9 Contour plots of the normalised squares of the (*a*) $2e_{1/2}$ (*xz* plane), (*b*) $3e_{1/2}$ (*xz* plane) and (*c*) $2e_{3/2}$ (σ_d plane) relativistic molecular orbitals of $[W(PH_3)_4O_2]$

As noted in the discussion of the non-relativistic calculations, there is a greater mixing of E and P character in many of the valence levels of $[W(PH_3)_4E_2]$ as E moves from Te to O. This is also found to be the case in the relativistic calculation on $[W(PH_3)_4O_2]$. There are significant oxygen contributions to the $4e_{1/2}$ and $3e_{3/2}$ W–P bonding orbitals, and the nominally O p_π lone-pair $5e_{1/2}$ and $4e_{3/2}$ MOs have 17.26 and 15.77% phosphorus content respectively.

Possibly the most significant difference between non-relativistic and relativistic calculations on $[W(PH_3)_4O_2]$ is the nature of the HOMO. The non-relativistic calculation has the $3a_1$ W–O bonding orbital slightly less stable than the $1b_2$ W $5d_{xy}$ MO, a situation which is reversed in the relativistic calculations. The latter restores the pattern, prevalent in

$[W(PH_3)_4E_2]$ (E = S or Te), of $[W(PH_3)_4E_2]$ being tungsten(IV) d^2 compounds.

(iv) Comparison of $[W(PH_3)_4O_2]$, $[W(PH_3)_4S_2]$ *and* $[W(PH_3)_4Te_2]$. Fig. 10 is the relativistic equivalent of Fig. 5, and compares the results of the relativistic calculations on $[W(PH_3)_4E_2]$ (E = O, S or Te). Many of the trends noted in the non-relativistic calculations are present in the relativistic case, in particular the marked destabilisation of the W–E bonding orbitals as the chalcogen becomes heavier. Also of note is the increased spin–orbit coupling in $[W(PH_3)_4Te_2]$, evidenced by the separation of the W–Te π-bonding $4e_{1/2}$ and $3e_{3/2}$ MOs, their π* counterparts, the $7e_{1/2}$ and $6e_{3/2}$, and in the energies and compositions of the $5e_{1/2}$–$4e_{3/2}$ levels. The HOMO is the W (5d + 5d̄) $5e_{3/2}$ orbital in all cases.

The trends in metal–chalcogen covalency discussed in the non-relativistic calculations are reproduced in the relativistic case. There is a significant increase in the tungsten content of the $3e_{1/2}$ MO as E moves from O to Te. This orbital is W–E σ bonding in $[W(PH_3)_4S_2]$ and $[W(PH_3)_4Te_2]$, although its σ/π nature is less clear cut in $[W(PH_3)_4O_2]$. The tungsten content of the π-bonding $4e_{1/2}$ and $3e_{3/2}$ levels once again remains much more constant as the chalcogen is altered.

(c) Comparison of the theoretical results on $[W(PH_3)_4E_2]$ (E = O, S *or* Te) *with the electronic absorption spectra of* $[W(PMe_3)_4E_2]$ (E = S, Se *or* Te). The electronic absorption spectra of $[W(PMe_3)_4E_2]$ (E = S, Se or Te) were recently reported.[15] They were interpreted in terms of an axially compressed ligand field, and it was found that the HOMO ⟶ LUMO (n ⟶ π*) transition ($1b_2$ ⟶ 4e in Figs. 1, 3 and 4; b_1 ⟶ e in the D_{2d} notation of ref. 15) increased in energy in the order Te < Se < S. Although ground-state Xα eigenvalues cannot be related directly to experimental transition energies, trends within them may be justifiably compared. The $1b_2$–4e gap increases from 1.26 eV in $[W(PH_3)_4Te_2]$ to 1.97 eV in $[W(PH_3)_4S_2]$ and 4.20 eV in $[W(PH_3)_4O_2]$, a trend which is mirrored in the relativistic equivalents.

Interestingly not one but two clearly resolved peaks are seen in the spectrum of $[W(PMe_3)_4Te_2]$, at 13 300 (1.65) and 14 900 cm^{-1} (1.85 eV). Two peaks are also found in the spectra of $[W(PMe_3)_4S_2]$ and $[W(PMe_3)_4Se_2]$, although their resolution is less good. These were interpreted in terms of a Jahn–Teller splitting of the ^1E state arising from the $(b_1)^1(e)^1$ configuration. An alternative explanation may be the spin–orbit splitting of the

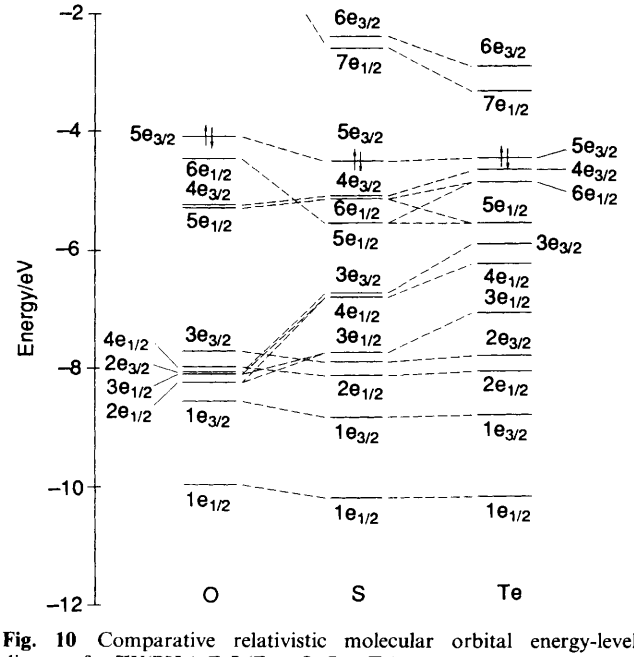

Fig. 10 Comparative relativistic molecular orbital energy-level diagram for $[W(PH_3)_4E_2]$ (E = O, S or Te)

4e MO into the $7e_{1/2}$ and $6e_{3/2}$ levels (Figs. 1 and 3), which provides two distinct transitions without the need to invoke Jahn–Teller distortions.

Also seen in the experimental spectra are ligand-to-metal charge-transfer transitions, which are formally π ⟶ π* in the metal–chalcogen double bond. These correspond to promotion of an electron from the 2e to the 4e MOs in Figs. 1, 3 and 4. They are again found experimentally to increase in energy from Te to S, which is mirrored in the calculational ground-state energy differences. In particular, it was noted that the failure to observe experimentally this π ⟶ π* transition in complexes where the multiply bonded ligand is a second-row element (*e.g.* =O, ≡CH, ≡N) arises because the ligand $2p_{xy}$ AOs lie too low in energy with respect to the metal $d_{xz,yz}$ level. This is supported by the calculation results on $[W(PH_3)_4O_2]$, in which the metal–chalcogen π bonding MO (the 1e level) is found to be significantly more stable than the equivalent orbital in $[W(PH_3)_4S_2]$ and $[W(PH_3)_4Te_2]$, to the extent that it lies below the $2a_1$ σ level [see above, section *(a) (ii)*]. Hence while the 2e–4e ground-state separation is 2.85 eV in $[W(PH_3)_4Te_2]$ and 4.21 eV in $[W(PH_3)_4S_2]$, it is 7.60 eV in $[W(PH_3)_4O_2]$, out of the range of optical spectroscopy.

Compounds $[Zr(TeSiH_3)_4]$ *and* ZrI_4.—The crystal structure of the recently synthesised $[Zr\{TeSi(SiMe_3)_3\}_4]$[4] shows that the $TeSi(SiMe_3)_3$ groups surround the Zr atom in a pseudo-tetrahedral array. There are some significant deviations in Te–Zr–Te bond angles from the tetrahedral angle, but is likely that these are caused primarily by interligand repulsions between the bulky $TeSi(SiMe_3)_3$ units. In the calculations reported here the $SiMe_3$ groups are replaced by H atoms and the structure idealised to T_d symmetry. It is unlikely that these changes will significantly alter the Zr–Te bonding.

The group $TeSiR_3$ may be considered isoelectronic with I as regards its interaction with the metal atom. The electronic structure of $[Zr(TeSiH_3)_4]$ is therefore expected to possess many of the features of that of ZrI_4. The electronic structure of the formally d^0 tetrahalides of the group IVA elements has been the subject of a number of both experimental[13,16–19,40–44] and theoretical[13,40,43,45–55] investigations. The large number of bands occurring in a narrow ionisation-energy range makes the photoelectron spectra of many of these molecules difficult to assign. This is due in no small part to the effects of spin–orbit coupling, the magnitude of which should be very similar for $[Zr(TeSiH_3)_4]$ and ZrI_4, as Te and I are neighbours in the Periodic Table. It was therefore decided to study both ZrI_4 and $[Zr(TeSiH_3)_4]$ in the hope that a comparison of the two molecules would yield more information than calculations on $[Zr(TeSiH_3)_4]$ alone.

(a) Non-relativistic calculations. In view of the many previous discussions of the valence electronic structure of d^0 MX_4 only a brief summary is provided here. The p orbitals of the halogens oriented along the M–X bond vectors (p_σ) decompose to a_1 + t_2 irreducible representations in T_d symmetry, while the p_π orbitals produce e + t_1 + t_2 combinations. The ordering of the resultant halogen p-based levels depends upon interhalogen repulsions and the interaction of the metal AOs with the ligand sets. Metal s content may be found in the a_1 level, p in the t_2 and d in both the t_2 and e. There is strictly no σ/π separation in the t_2 levels. In the absence of metal f orbitals, the t_1 ligand combination is rigorously non-bonding.

The results of a non-relativistic DV-Xα calculation on ZrI_4 are given on the left-hand side of Fig. 11. The $1a_1$–$1t_1$ MOs are the halogen-based orbitals outlined above, while the 2e and $3t_2$ levels are predominantly metal 4d in character. They correspond to the well known two-below-three splitting of metal d orbitals in a tetrahedral ligand field.[36] The MOs are filled up to and including the $1t_1$, in accord with the formal description of ZrI_4 as a d^0 molecule. Of the $1a_1$–$2t_2$ MOs, zirconium contributions range from a small (5.82%) 5s content to the $1a_1$ level to more substantial 4d character in the $1t_2$ and 1e orbitals

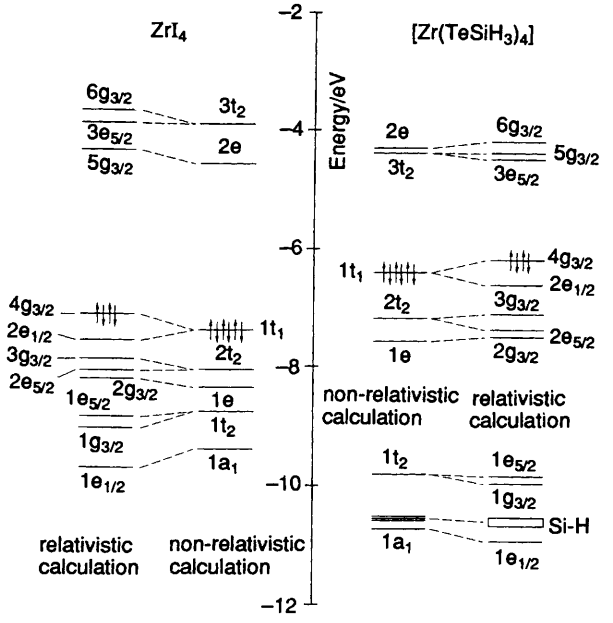

Fig. 11 Non-relativistic and relativistic molecular orbital energy-level diagrams for ZrI_4 and $[Zr(TeSiH_3)_4]$

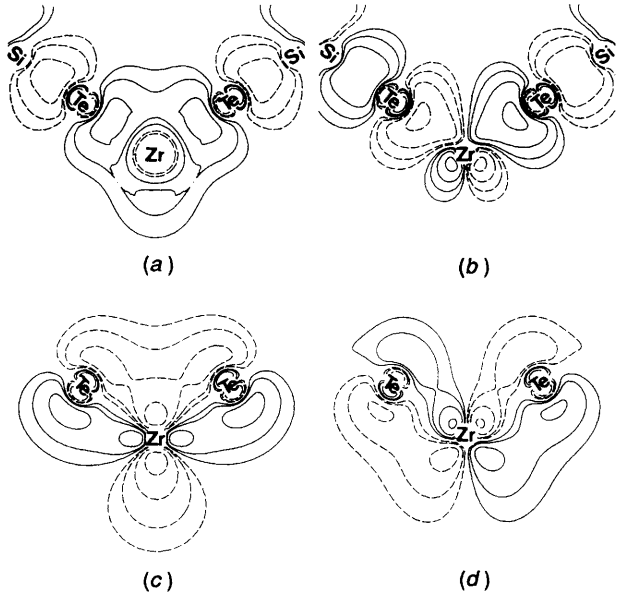

Fig. 12 Contour plots of the (*a*) $1a_1$, (*b*) $1t_2$, (*c*) 1e and (*d*) $2t_2$ molecular orbitals of $[Zr(TeSiH_3)_4]$, viewed in one of the σ_d planes

(24.58 and 28.81% respectively). The metal contributions to and ordering of the $1a_1$–$1t_1$ levels are very similar to those found in an equivalent calculation on $TiCl_4$.[13]

The right-hand side of Fig. 11 gives the non-relativistic results obtained on $[Zr(TeSiH_3)_4]$, and Fig. 12 presents contour plots of the $1a_1$, $1t_2$, 1e and $2t_2$ orbitals. Although the ordering of the $1a_1$–$1t_1$ MOs is the same as in ZrI_4 there are significant differences in their energies. The $1a_1$ and $1t_2$ levels are stabilised with respect to those of their ZrI_4 analogues, while the 1e–$1t_1$ MOs are destabilised. As the $1a_1$ and $1t_2$ have predominant σ character and the 1e–$1t_1$ possess π symmetry (Fig. 12), replacement of I by $TeSiH_3$ results in an energetic separation of the σ and π levels. In ZrI_4 the $1t_2$ MO is 0.36 eV more stable than the 1e whereas in $[Zr(TeSiH_3)_4]$ the gap is over six times larger at 2.25 eV. This has important consequences for spin–orbit coupling in the t-symmetry subshells of ZrI_4 and $[Zr(TeSiH_3)_4]$ [see below, section (*b*)].

The $1t_1$ MO has no metal content. In ZrI_4, therefore, it is 100% I 5p in character and in $[Zr(TeSiH_3)_4]$ it is still almost exclusively Te 5p-based (93.86%). If the interligand repulsions in ZrI_4 and $[Zr(TeSiH_3)_4]$ are assumed to be similar, the energy of the $1t_1$ orbital reflects the energy of the I and Te 5p AOs in the complex. The I 5p AOs are found to be 0.99 eV more stable than those of Te.

The metal and I/Te content of the 1e and $2t_2$ MOs may also be compared between ZrI_4 and $[Zr(TeSiH_3)_4]$, as they are found to have negligible Si and H character in the latter. In both orbitals there is a slightly greater zirconium content in $[Zr(TeSiH_3)_4]$, the 1e level being approximately one third metal d in character. Fig. 12(*c*) and 12(*d*) illustrate the significant metal contributions to the 1e and $2t_2$ MOs, and suggest that the formal description of $[Zr(TeSiH_3)_4]$ and ZrI_4 as singly bonded molecules is misleading. Both the 1e and $2t_2$ MOs are metal–ligand π bonding, the 1e MO rigorously so by symmetry.

The $1a_1$ and $1t_2$ levels of $[Zr(TeSiH_3)_4]$ are delocalised over all of the molecule, with significant Si–H and Si–Te bonding character in addition to Zr–Te. Given that the 1e–$1t_1$ MOs (which have no Si or H content) have less-negative eigenvalues in $[Zr(TeSiH_3)_4]$ than in ZrI_4, it is likely that the Si and H character of the $1a_1$ and $1t_2$ orbitals contributes toward their stabilisation. Indeed, the $1a_1$ orbital is found to be more stable than some of the Si–H bonding levels. The zirconium content of the $1a_1$ and $1t_2$ MOs is about the same in $[Zr(TeSiH_3)_4]$ and ZrI_4, but is distributed differently. There is a greater 5s content to the $1a_1$ level in the tellurium compound, with a reduction in the 4d character of the $1t_2$.

The ordering of the unoccupied $3t_2$ and 2e orbitals in $[Zr(TeSiH_3)_4]$ is interesting in that it is reversed from that in ZrI_4 and from that expected on the basis of simple crystal-field theory. The 2e and $3t_2$ MOs of ZrI_4 are the metal–halogen antibonding counterparts of the 1e and $1t_2$ levels. In $[Zr(TeSiH_3)_4]$ the effect of the Si is to distort the usual e-below-t_2 splitting. The marked stabilisation of the bonding $1t_2$ orbital carries through to the unoccupied $3t_2$, giving it a more negative eigenvalue than that of the 2e.

(*b*) *Relativistic calculations: spin–orbit coupling in the t symmetry MOs.* The results of the relativistic calculations on ZrI_4 and $[Zr(TeSiH_3)_4]$ are given in Fig. 11. Table 1 provides the relationship between the spatial MOs of T_d and the spin orbitals of T_d^*, from which it may be seen that the degeneracy of the t-symmetry MOs is lifted in the double group.

In both molecules the $1e_{1/2}$ level is stabilised over the $1a_1$ non-relativistic orbital. This is most likely due to its Zr 5s contribution, for the reasons given earlier. Similarly the 4d content of the $2g_{3/2}$ MOs is responsible for their destabilisation over their non-relativistic analogues.

Spin–orbit coupling in the t-symmetry subshells of tetrahedral halides has been a subject of interest for over 20 years.[16–19] The current calculations provide an opportunity to test some of the conclusions drawn from earlier studies. Assuming the spin–orbit coupling to be due solely to the halogen atoms, it was predicted that the magnitude of t-orbital splitting should be $(3/2)\zeta_t$,[16] where ζ_t is the spin–orbit coupling constant for the t MO of interest. The ordering of the spin–orbit split components was found to be $g_{3/2} < e_{1/2}$ for the $t_1(\pi)$ orbitals (*i.e.* $g_{3/2}$ has a less negative eigenvalue), $g_{3/2} < e_{5/2}$ for the $t_2(\pi)$ but $e_{5/2} < g_{3/2}$ for $t_2(\sigma)$ levels. Furthermore the magnitude of the $t_2(\pi)$ splitting was predicted to be approximately twice that of the $t_2(\sigma)$.

In both ZrI_4 and $[Zr(TeSiH_3)_4]$ the $1t_2$ $[t_2(\sigma)]$, $2t_2$ $[t_2(\pi)]$ and $1t_1$ $[t_1(\pi)]$ MOs split in the relativistic calculations into levels whose ordering is consistent with the above predictions. The separation of the $2e_{1/2}$ and $4g_{3/2}$ orbitals is similar in both cases, at 0.43 eV in ZrI_4 and 0.39 eV in $[Zr(TeSiH_3)_4]$. The *ca.* 6.5% combined (Si + H) contribution to the $2e_{1/2}$ and $4g_{3/2}$

levels of $[Zr(TeSiH_3)_4]$ may be responsible for slightly reduced splitting.

The separation of the relativistic levels derived from the t_2 MOs is noticeably different in the two compounds. In ZrI_4 the energy gap between the $1g_{3/2}$ and $1e_{5/2}$ MOs is 0.19 eV, which is almost identical to that between the $2e_{5/2}$ and $3g_{3/2}$ levels (0.20 eV). In $[Zr(TeSiH_3)_4]$, however, the separation of the $t_2(\sigma)$ spin–orbit coupled levels is only 0.12 eV, while the $2e_{5/2}$ and $3g_{3/2}$ orbitals are split by 0.28 eV. It would therefore appear that $[Zr(TeSiH_3)_4]$ is in closer agreement with the prediction of the magnitude of the t_2 subshell spin–orbit splittings than is ZrI_4.

It must be emphasised that the predicted splittings are derived from ligand-based spin–orbit coupling only. This raises the question as to whether the differences between ZrI_4 and $[Zr(TeSiH_3)_4]$ arise from metal contributions to the t_2 levels. Although the zirconium content of the $1g_{3/2}$, $1e_{5/2}$, $2e_{5/2}$ and $3g_{3/2}$ orbitals is smaller than the I/Te, it is conceivable that it is sufficient to cause the observed separation differences.

The Zr (4d + 4$\bar{d}$) character in the $2e_{5/2}$ and $3g_{3/2}$ levels will reduce their separation, as metal d-derived splitting produces an $e_{5/2} < g_{3/2}$ ordering.[30] There is a slightly *greater* Zr (4d + 4$\bar{d}$) contribution to the $2e_{5/2}$ and $3g_{3/2}$ MOs of $[Zr(TeSiH_3)_4]$ than to ZrI_4 (11.34 and 19.06% *vs.* 3.59 and 15.86% respectively), and yet their separation is almost 50% larger. Conversely Zr (5p + 5$\bar{p}$) content in the $t_2(\pi)$-derived orbitals will reinforce their splitting,[30] and yet there is more metal p character in the $2e_{5/2}$ and $3g_{3/2}$ MOs of ZrI_4 {ZrI_4 $2e_{5/2}$ 6.21% 5$\bar{p}$, $3g_{3/2}$ 3.07% 5p; $[Zr(TeSiH_3)_4]$ $2e_{5/2}$ 3.01% 5$\bar{p}$, $3_{3/2}$ 1.81% 5p}. Metal-based spin–orbit coupling arguments are thus at a loss to explain the $t_2(\pi)$ splittings.

In contrast, Zr (4d + 4$\bar{d}$) character to the $1g_{3/2}$ and $1e_{5/2}$ MOs will reinforce their separation, and indeed there is greater (4d + 4$\bar{d}$) content in the $t_2(\sigma)$ levels of ZrI_4, in accord with their greater splitting. Overall, however, two factors mitigate against the differences in t_2 subshell spin–orbit splittings being due to zirconium content. Not only are the metal contributions comparatively small, but it is unsatisfactory to have them explain the greater $t_2(\sigma)$ separation in ZrI_4 and yet be completely at odds with the $t_2(\pi)$ splittings.

There is another possible explanation which avoids the need to invoke metal-based arguments. The energy separation of the $1t_2$ and $2t_2$ non-relativistic MOs of ZrI_4 is 0.70 eV, while the equivalent gap in $[Zr(TeSiH_3)_4]$ is 2.60 eV, nearly four times greater. The separation of the $2e_{1/2}$ and $4g_{3/2}$ levels may be taken as a guide to the magnitude of ligand-based spin–orbit coupling in both molecules, as these orbitals have virtually no metal character. Hence the separation of the $1t_2$ and $2t_2$ MOs of ZrI_4 is seen to be less than twice the spin–orbit coupling of the I-based $1t_1$ orbital. In $[Zr(TeSiH_3)_4]$, however, the gap between the $1t_2$ and $2t_2$ levels is nearly seven times the splitting of the $2e_{1/2}$ and $4g_{3/2}$ orbitals. This raises the question as to whether it is valid to differentiate between $t_2(\sigma)$ and $t_2(\pi)$ orbitals in ZrI_4, for it is likely that appreciable σ/π mixing will occur in their relativistic orbitals on account of their proximity in energy. This is less likely to happen in $[Zr(TeSiH_3)_4]$ as the $1t_2$ and $2t_2$ [and hence $(1g_{3/2} + 1e_{5/2})$ and $(2e_{5/2} + 3g_{3/2})$] MOs are so much further apart in energy.

Fig. 13 indicates that this is a correct assertion. While the $1g_{3/2}$ MO of $[Zr(TeSiH_3)_4]$ is seen to be σ in character and the $3g_{3/2}$ π, the equivalent levels of ZrI_4 have both σ and π contributions. This conclusion elegantly rationalises the spin–orbit splittings of the $1t_2$ and $2t_2$ levels of ZrI_4 and has important consequences for the interpretation of the photoelectron spectra of the Group IVA tetrahalides. The model spin–orbit splittings are shown to break down when the magnitude of spin–orbit coupling becomes comparable with the separation of the '$t_2(\sigma)$' and '$t_2(\pi)$' levels, and the resulting relativistic orbitals have both σ and π character. The compound $[Zr(TeSiH_3)_4]$ would suggest that the predictions are more accurate when the $t_2(\sigma)$ and $t_2(\pi)$ levels are well separated in energy. It is ironic that the electronic structure of $[Zr(TeSiH_3)_4]$ is more like that predicted for a tetrahalide than is that of ZrI_4.

(*c*) *Metal–tellurium covalency in* $[W(PH_3)_4Te_2]$ *and* $[Zr(TeSiH_3)_4]$. Caution must be exercised when comparing the metal–ligand bonding in $[W(PH_3)_4Te_2]$ and $[Zr(TeSiH_3)_4]$ as there are significant differences between the two compound types. The former has ancillary ligands and terminal Te atoms, whereas the Te atoms in the latter are bound to Si in addition to the metal. One possible approach is to compare the amount of metal character in the MOs responsible for binding the metal to Te. In $[W(PH_3)_4Te_2]$ these are the $2a_1$, 2e and $3a_1$ orbitals while Fig. 12 indicates that Zr–Te bonding character is present in the $1a_1$–$2t_2$ MOs of $[Zr(TeSiH_3)_4]$. (The percentage of metal and ligand character in the relativistic equivalents of these MOs is little altered from the non-relativistic, and hence comparison of the non-relativistic compositions is valid.) The tungsten character per orbital in the $2a_1$, 2e and $3a_1$ of $[W(PH_3)_4Te_2]$ is 35.92%, while in $[Zr(TeSiH_3)_4]$ the zirconium content per orbital of the $1a_1$, $1t_2$, 1e and $2t_2$ is only 20.52%. There is therefore seen to be significantly greater metal contributions to the metal–ligand bonding MOs in $[W(PH_3)_4Te_2]$ than in $[Zr(TeSiH_3)_4]$.

There is a number of possible interpretations of/explanations for this. Generally the most ionic compounds are those formed between elements from opposite sides of the Periodic Table, those with the greatest electronegativity differences. The Allred–Rochow electronegativities of Zr, W and Te are 1.22, 1.40 and 2.40 respectively,[31] suggesting that $[W(PH_3)_4Te_2]$ should be more covalent than $[Zr(TeSiH_3)_4]$. A related approach is to examine the energies of the principal valence AOs of the three elements. Table 2 provides the results of non-relativistic and relativistic Hartree–Fock calculations on atomic Zr, W and Te, using the method of Cowan.[32] The energy separation of the W 5d and the Te 5p AOs is only 0.41 eV (relativistic calculation) while that of the Te 5p/Zr 4d is 1.59 eV. Greater covalency may therefore be expected in the tungsten compound.

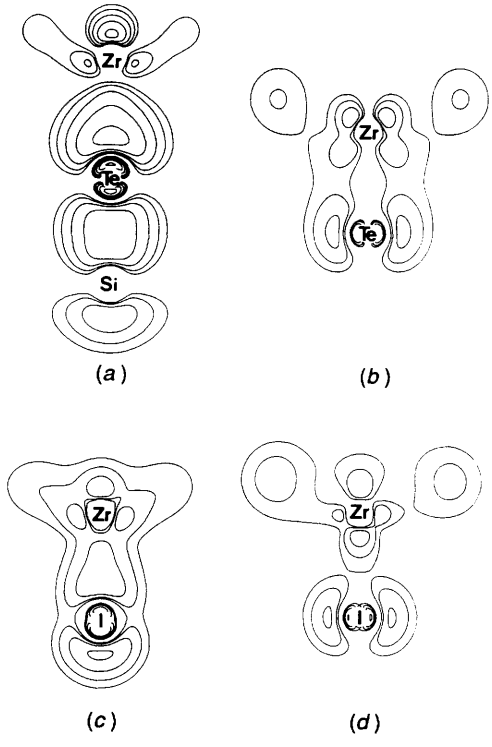

Fig. 13 Contour plots of the normalised squares of the (*a*) $1g_{3/2}$ and (*b*) $3g_{3/2}$ relativistic molecular orbitals of $[Zr(TeSiH_3)_4]$ and (*c*) $1g_{3/2}$ and (*d*) $3g_{3/2}$ relativistic molecular orbitals of ZrI_4, viewed in a plane containing only one metal–ligand bond

Table 2 Valence atomic orbital energies (eV) of Zr, W and Te obtained from non-relativistic and relativistic Hartree–Fock calculations[32]

Atomic orbital	Non-relativistic calculation	Relativistic calculation
Zr 4d	−8.46	−7.92
W 5d	−10.96	−9.10
Te 5p	−9.54	−9.51

Acknowledgements

I thank the SERC/NATO for a postdoctoral fellowship, and Dr. Jennifer Green and Professor Bruce Bursten for helpful discussions. This work was supported by the Division of Chemical Sciences, Office of Basic Energy Sciences, US Department of Energy (Grant DE-FG02-86ER13529).

References

1 W. A. Nugent and J. M. Mayer, *Metal-Ligand Multiple Bonds*, Wiley-Interscience, New York, 1988.
2 E. W. Harlan and R. H. Holm, *J. Am. Chem. Soc.*, 1990, **112**, 186 and refs. therein.
3 P. O'Brien, *Chemtronics*, 1991, **5**, 61.
4 V. Christou and J. Arnold, *J. Am. Chem. Soc.*, 1992, **114**, 6240.
5 W. A. Herrmann, *Angew. Chem., Int. Ed. Engl.*, 1986, **25**, 56.
6 N. A. Compton, R. J. Errington and N. C. Norman, *Adv. Organomet. Chem.*, 1990, **31**, 91.
7 D. Rabinovich and G. Parkin, *J. Am. Chem. Soc.*, 1991, **113**, 9421.
8 D. Rabinovich and G. Parkin, *J. Am. Chem. Soc.*, 1991, **113**, 5904.
9 G. Parkin, personal communication.
10 D. E. Ellis, *J. Phys. B*, 1977, **10**, 1.
11 W. F. Schneider, Ph.D. Dissertation, Ohio State University, 1991.
12 W. F. Schneider, R. J. Strittmatter, B. E. Bursten and D. E. Ellis, *Density Functional Methods in Chemistry*, Springer, New York, 1991, ch. 16.
13 B. E. Bursten, J. C. Green, N. Kaltsoyannis, M. A. MacDonald, K. H. Sze and J. S. Tse, *Inorg. Chem.*, in the press.
14 B. E. Bursten, J. C. Green and N. Kaltsoyannis, *Inorg. Chem.*, in the press.
15 J. A. Paradis, D. W. Wertz and H. H. Thorp, *J. Am. Chem. Soc.*, 1993, **115**, 5308.
16 J. C. Green, M. L. H. Green, P. J. Joachim, A. F. Orchard and D. W. Turner, *Philos. Trans. R. Soc. London, Ser. A*, 1970, **268**, 111.
17 R. G. Egdell, D. Phil. Thesis, Oxford, 1977.
18 R. G. Egdell and A. F. Orchard, *J. Chem. Soc., Faraday Trans. 2*, 1978, 485.
19 N. Kaltsoyannis, D.Phil. Thesis, Oxford, 1992.
20 P. Pyykkö, *Acc. Chem. Res.*, 1979, **8**, 276.
21 J. A. Salthouse and M. J. Ware, *Point Group Character Tables and Related Data*, Cambridge University Press, London, 1972.
22 I. P. Grant, *Adv. Phys.*, 1970, **19**, 747.
23 I. P. Grant, *Methods in Computational Chemistry*, Plenum, New York, 1988, vol. 2, ch. 1.
24 J. S. Slater, *Phys. Rev.*, 1951, **81**, 385.
25 J. C. Slater, *Adv. Quantum Chem.*, 1972, **6**, 1.
26 L. Hedin and B. I. Lundqvist, *J. Phys. C*, 1971, **4**, 2064.
27 B. Delley and D. E. Ellis, *J. Chem. Phys.*, 1982, **76**, 1949.
28 R. S. Mulliken, *J. Chem. Phys.*, 1955, **23**, 1833, 1841, 2338, 2343.
29 F.-M. Su, C. Cooper, S. J. Geib, A. L. Rheingold and J. M. Mayer, *J. Am. Chem. Soc.*, 1986, **108**, 3545.
30 J. C. Green, M. F. Guest, I. H. Hillier, S. A. Jarrett-Sprague, N. Kaltsoyannis, M. A. MacDonald and K. H. Sze, *Inorg. Chem.*, 1992, **31**, 1588.
31 J. E. Huheey, *Inorganic Chemistry*, 3rd edn., Harper and Row, New York, 1983.
32 R. D. Cowan, *The Theory of Atomic Structure and Spectra*, Chemical Abstracts Service, Columbus, OH, 1981.
33 C. J. Ballhausen and H. B. Gray, *Inorg. Chem.*, 1962, **1**, 111.
34 J. K. Winkler and H. B. Gray, *Inorg. Chem.*, 1985, **24**, 346.
35 C. S. Johnson, C. Mottley, J. T. Hupp and G. D. Danzer, *Inorg. Chem.*, 1992, **31**, 5143.
36 N. N. Greenwood and A. Earnshaw, *Chemistry of the Elements*, Pergamon, Oxford, 1984, ch. 19.
37 P. Pyykkö, J. Li, T. Bastug, B. Fricke and D. Kolb, *Inorg. Chem.*, 1993, **32**, 1525.
38 C. E. Moore, *Atomic Energy Levels, NSRDS-NBS 35*, 1971, **1**.
39 P. W. Atkins, *Molecular Quantum Mechanics*, Oxford University Press, Oxford, 1983.
40 P. Burroughs, S. Evans, A. Hamnett, A. F. Orchard and N. V. Richardson, *J. Chem. Soc., Faraday Trans. 2*, 1974, 1895.
41 R. G. Egdell, A. F. Orchard, D. R. Lloyd and N. V. Richardson, *J. Electron Spectrosc. Relat. Phenom.*, 1977, **12**, 415.
42 P. A. Cox, S. Evans, A. Hamnett and A. F. Orchard, *Chem. Phys. Lett.*, 1970, **7**, 414.
43 G. M. Bancroft, E. Pellach and J. S. Tse, *Inorg. Chem.*, 1982, **21**, 2950.
44 H. E. Wetzel, Ph.D. Thesis, Hamburg, 1987.
45 C. A. L. Becker and J. P. Dahl, *Theor. Chim. Acta*, 1969, **14**, 26.
46 C. A. L. Becker, C. J. Ballhausen and I. Trajberg, *Theor. Chim. Acta*, 1969, **13**, 355.
47 F. Choplin and G. Kaufmann, *Theor. Chim. Acta*, 1972, **25**, 54.
48 D. R. Truax, J. A. Geer and T. Ziegler, *J. Chem. Phys.*, 1973, **59**, 6662.
49 F. R. Fenske and D. D. Radtke, *Inorg. Chem.*, 1968, **7**, 479.
50 D. E. Ellis and T. Parameswan, *Int. J. Quantum Chem., Symp.*, 1971, **5**, 443.
51 T. Parameswan and D. E. Ellis, *J. Chem. Phys.*, 1973, **58**, 2088.
52 J. A. Tossell, *Chem. Phys. Lett.*, 1979, **65**, 371.
53 A. E. Foti, V. H. Smith and M. A. Whitehead, *Mol. Phys.*, 1982, **45**, 385.
54 I. H. Hillier and J. Kendrick, *Inorg. Chem.*, 1976, **15**, 520.
55 W. von Niessen, *Inorg. Chem.*, 1987, **26**, 567.

Received 8*th November* 1993; *Paper* 3/06677K